Project ID: Fly-Radar

Project Title: Low-frequency multi-mode (SAR and penetrating) radar onboard light-weight UAV for Earth and Planetary exploration

Call: H2020-MSCA-RISE-2020

WP1 –
Mars Surface and subsurface analyses and terrestrial analogs

D1.1: Preliminary Mars Environmental Description for Scientific Requirements Engineering

Lead contributor	UCBL (4 – Université Claude Bernard Lyon 1)
Other contributors	CSFK (3 – CSILLAGASZATI ES FOLDTUDOMANYI KUTATOKOZPONT)
	CBK PAN (2 - CENTRUM BADAN KOSMICZNYCH POLSKIEJ AKADEMII NAUK) -
	Ud'A (7 - UNIVERSITA DEGLI STUDI GABRIELE D'ANNUNZIO DI CHIETI-PESCARA)

Due date	31 May 2021
Delivery date	15 July 2021
Deliverable type	Report[1]
Dissemination level	PU

Document History

Version	Date	Description
V1.0	31 May 2021	Final
V2.0	06 September 2021	Final (Revision)

This project has received funding from the European Union's Horizon 2020 research and innovation programme under MSCA-RISE2020 grant agreement No 101007973.

1. Publishable Summary

The aim of FlyRadar is to develop and test a drone carrying a Synthetic Aperture Radar (SAR) and Ground Penetrating Radar (GPR) able to provide images of the subsurface. The GPR will be dimensioned for the Martian environment. A GPR is an active remote sensing probe that emits electromagnetic waves and receives the waves reflected by discontinuities that can be the surface of the planet or layers in the interior. The analysis of these echoes provides geometrical and some geological information on the surface and on the layering to depth that depends on the material and that never exceeds for such an instrument about 100 m. The upper crust of Mars is composed by rocks of various origins (volcanic, sedimentary, alteration, etc.), clearly visible at the surface of the planet. Mars also presents two permanent polar caps and a range of various shallow subsurface buried snow and ice masses in the middle latitude region. The shallow subsurface 3D geometry of these geological features is generally poorly known, however will be accessible by a GPR-SAR instrument. The efficiency of GPR has already been demonstrated on Mars. Two GPR (Marsis on Mars Express and Sharad on MRO) have operated from satellite platforms in the last 20 years. These two instruments provided the first images of the subsurface of Mars. The FlyRadar improved system that will operate at few tenth of m in elevation onboard a drone will provide more precise and resolute data, what are inevitable for future Mars Sample Initiatives, and the planned human mission.

2. Introduction

This deliverable describes the preliminary work done in frame of the WP1 of Fly Radar Project. This WP1, entitled "**Scientific aims for Mars Surface analyses and Terrestrial analogues"**, is a scientific work package whose goal is establishing knowledge and models of the Mars surface and subsurface environment with regards to those parameters affecting radar investigations by other WPs.

Mars is the fourth planet of the solar system. It is the most studied planet after the Earth, and presents a range of similarity to Earth, including volcanoes, fluvial valleys, glacier-like features, aeolian dunes, weathered minerals etc., and the possibility of extinct or extant life. These complex aspects require sophisticated technology to analyse them, what support innovation and a leading role in the technology development of planetary exploration, including the radar based topics targeted by this project. Since the middle of the 60', Mars has been explored by orbiting probes carrying scientific instruments, by landers and rovers which analysed the Martian surface and provided data to study Mars interior. Among these instruments, 2 radars similar to those developed in the frame of the FlyRadar project were deployed on orbiters during the last 20 years. In the first years of 2000', the Marsis radar (Jordan et al., 2009) on board of "Mars Express" had the objective to map the distribution of water and ice in the upper portions of the Martian crust. Ten years later, the SHARAD (Shallow Radar) radar (Seu et al., 2007) on board the "Mars Reconnaissance Orbiter" (MRO) had a similar objective with a better spatial resolution.

Radar systems emit electromagnetic signals from a few MHz to several tens of GHz toward the ground. At these frequencies, the rocks and the ice are partially transparent. The signal can thus penetrate these levels and possibly be reflected on dielectric discontinuities of the subsurface. This method of non-destructive probing was first deployed from systems installed on the ground and used in archaeology, glaciology, civil engineering or mining prospecting. The first sounder radar installed on a satellite was deployed around the Moon (Porcello et al., 1974). Other similar systems have been carried on satellites to study comet 67P - C G, Mars, the Moon. Earth is not an ideal target for this type of instrument. In fact, the electromagnetic signal

This project has received funding from the European Union's Horizon 2020 research and innovation programme under MSCA-RISE2020 grant agreement No 101007973.

is rapidly absorbed by liquid water, which is very common in the surface levels of land areas. Mars is currently characterized by a very low water content on its surface and below it. Radar is therefore a privileged tool for studying its subsurface.

The work reported in the present document consists in (1) a description of the parameters of radar, (2) a description of the main geological objects that can be found on Mars and (3) the possible range of the geological and environmental parameters of the Martian surface and subsurface.

3. Overview of radar capabilities

A radar is an active remote sensing system that works similarly to echography. A beam of energy is sent toward the target to investigate. Part of the beam is reflected by the various surfaces and discontinuities the signal has been went through. The reflected part of the beam (the echo) is registered by the sensor in term of delay since the emission, signal intensity and possibly signal phase. Evaluating the received signal it is possible to measure the distance between the source and the target from the echo received by the sensor. It is also possible to estimate the properties of the medium the beam went through, the speed of the signal in such materials and possibly the nature of the material. Whilst the echography uses soundwaves, the radar uses electromagnetic waves to make its measures. For the study of planetary surfaces, radars can register the echo from the surface to provide a image of the surface, or radars can register echoes of the signal that crossed the planetary surface and was reflected by interfaces of the basement. In that case the radar operates in “Ground Penetrating Radar” mode.

3.1 Synthetic Aperture Radars

A classic radar emits a single pulse of energy in a given direction, and measures the delay to the reception of the echoed back pulse. From this delay the distance from the discontinuity that creates the echo is measured. In practice, the radio signal is not absolutely directive but has a given angular aperture that depends on the antenna which is used. This aperture implies that the radar not only receives echoes directly from the pointing emission direction but also from directions slightly off the pointing direction. From this kind of basic radar, it is impossible to discriminate the echo direction. The SAR (Synthetic Aperture Radar) is a radar mounted on a moving platform relative to the target. This platform can be a satellite, a plane or a drone for example. The relative speed between the radar and its target induces a Doppler shift on the received echo. Such shift can be used to discriminate between an echo from the nadir and an echo from an object located along the track of the radar. This method cannot discriminate two points that are aligned in the direction perpendicular to the movement of the platform.

3.2 Radar Components

The firsts generations or radars were built to operate at frequencies chosen for a given type of application, such as body detection, fume detection or vegetation scanning. Only after the 1990s and the birth of SDR (Software Defined Radio) radars became more versatile, able to operate at different frequencies, over different bandwidth, without requiring to change electronics. In a SDR radar substitutes some part of the hardware components are replaced (filter, modulators, generators) by software components built into a Field Programmable Gate Array (FPGA) that acts as the ’reprogrammable’ version of the hardware components (Cerquera et al., 2017, Ferro, 2011). Nowadays SDR is commonly used and will be employed for the RISE project.

A radar using the SDR technology consists in four main parts:

This project has received funding from the European Union’s Horizon 2020 research and innovation programme under MSCA-RISE2020 grant agreement No 101007973.

• The antenna(s): Obviously, a radar needs an antenna to emit and receive radio signals. Monostatic radars use only one antenna which periodically switches between emitting and receiving mode. Bistatic radar uses two distinct antennas. One is dedicated to emission, the other to reception.

• The SDR system: This system handles the signal generation and reception. It contains the programmable FPGA, which will contain the code that defines the operating modes.

• The Power System: The signal generated by the SDR system has to be amplified to be emitted by the antenna. The amplification is made by the power system.

• The Data Management System: Data sent and received are processed and stored by the Data Management System that is similar to a rational computer.

3.3 Radar Resolution

Radar parameters that are important for the study of planetary surfaces and interiors, are the vertical and horizontal resolution, which indicate the capacity of the instrument to discriminate 2 different points at the surface or two different interfaces in the interior.

• Over the vertical axis, the depth resolution of a penetrating radar is the minimal vertical distance between two discontinuities the radar will be able to distinguish.

• Over the direction perpendicular to the movement of the radar, one can define the across-track resolution that is the minimal distance along the direction perpendicular to the movement of two reflectors that can be separated by the radar

• Over the direction of the movement of the radar, one can define the along-track resolution. This resolution is better than the across-track resolution thanks to synthetic aperture post-processing.

3.3.1 Vertical Resolution

The signal emitted by the radar is polychromatic around a central frequency over a given bandwidth B_w. The depth resolution (or range resolution) δz is:

$$\delta_z = \frac{c}{2B_w\sqrt{\varepsilon_r}} \text{ (eq. 1)}$$

Where, c is the speed of light and ε_r is the relative permittivity of the material in which the signal propagates.

3.3.2 Along-track Resolution

The Doppler processing permitted by the SAR technics improves greatly the along track resolution of a radar. Unfocused or Focused Processing of the signal can be realized. The Unfocussed processing requires less resource.

3.3.2.1 Focused Processing

In the case of a Focused processing, the resolution depends on the Doppler bandwidth B_D, which is the bandwidth of the shift caused by the Doppler effect:

$$B_D = \frac{2V^2}{h\lambda_c} t_i \text{ (eq. 2)}$$

This project has received funding from the European Union's Horizon 2020 research and innovation programme under MSCA-RISE2020 grant agreement No 101007973.

Where V and h are the speed and the height of the platform, λ_c the central wavelength of the signal emitted by the radar and t_i the integration time of the radar, i.e. the time during which a single point is illuminated by the radar. For a target located at a distance R from the drone, the integration time is given by:

$$t_i = \theta_{3dB} \frac{h}{V} \text{ (eq. 3)}$$

Where, θ_{3dB} is the aperture of the radar antenna at 3dB. The along track resolution of the Focused processing is:

$$\delta_{x,Focussed} \approx \frac{V}{B_D} \approx \frac{\lambda_c}{\theta_{3dB}} \text{ (eq. 4)}$$

3.3.2.2 Unfocused Processing

The Unfocused Processing does not use the whole signal bandwidth and considers the radar pulse as monochromatic. The integration time in that case is:

$$t_{i,eff} = \frac{1}{V_s} \sqrt{\frac{h\lambda_c}{2}} \text{ (eq.5)}$$

The resulting along-track resolution is:

$$\delta_{x,Unocussed} \approx \sqrt{\frac{h\lambda_c}{2}} \text{ (eq.6)}$$

The resolution of the unfocussed processing is larger than the resolution provided by focused processing

3.3.3 Across-track Resolution

The across-track resolution has two distinct definitions, according the reflective surface is considered smooth or rough. A surface is considered as smooth if it roughness is small compared to the wavelength of the radar signal (Grima, 2011).

3.3.3.1 Smooth Surface

The across track resolution of the radar on a smooth surface is equal to the diameter of the first Fresnel zone:

$$\delta_y^{smooth} = \sqrt{2\lambda_c h} \text{ (eq. 7)}$$

3.3.3.2 Rough Surface

In the case of a rough surface, the across track resolution is given by the diameter of the pulse limited resolution cell, that is the intersection between the radar wave front and the surface when a part of this wave front has already traveled a distance equal to the vertical resolution of the radar:

$$\delta_y^{rough} = 2\sqrt{2h\delta_z} = 2\sqrt{\frac{hc}{B_w}} \text{ (eq. 8)}$$

This project has received funding from the European Union's Horizon 2020 research and innovation programme under MSCA-RISE2020 grant agreement No 101007973.

3.3.4 Side Looking SAR

In the case of a side looking radar (which is a common configuration for SARs), the previously defined depth resolution must be seen as the resolution in the direction of the radar. The resulting depth resolution is equal to the projection of the former resolution on a vertical axis.

3.4 Radar Operating Frequency

3.4.1 Main Radar Frequency Ranges

The main radar frequency ranges are summed up in table 1. In the case of the RISE project, we are mostly interested into GPR (Ground Penetrating Radar), which uses frequencies typically between 1 and 1000 MHz.

Table 1: Radio Frequency bands used by radars and their applications. (GPR: Ground Penetrating Radar).

Band name	Frequency range	Description
HF	3-30 MHz	Coastal radar systems
VHF	30-300 MHz	GPR
UHF	300-1000 HMz	GPR, very long range surveillance
L	1-2 GHz	Long range surveillance)
S	2-4 GHz	Moderate range surveillance
C	4-8 GHz	Weather, long range tracking
X	8-12 GHz	Marine radar, weather, mapping, short range tracking
K_u	12-18 GHz	Mapping
K	18-24 GHz	Weather (cloud detection)
K_a	24-40 GHz	Mapping, short range surveillance
V	40-75 GHz	Atmospheric oxygen absoption, not used
W	75-110 GHz	Weather, imaging, tracking

3.4.2 GPR Radar

The operating frequency that could maximize the penetration depth into the ground (or probing distance) is controlled by 4 parameters [4] that are:

- The spreading attenuation of the electromagnetic wave. In case of a spherical wave front, the attenuation follows the inverse-square law. A scattering attenuation that occurs when the wave front hits a heterogeneous surface is added to the spreading attenuation.
- The ground material's absorption of the electromagnetic energy.
- The intensity of the reflection of the electromagnetic wave onto the discontinuity.
- The sensitivity, or performance, of the radar reception.

The amplitude of an incoming electromagnetic wave decreases exponentially as the wave penetrate the ground:

$$A(x) = Aoe^{-\alpha x} \text{ (eq. 9)}$$

where x is the distance traveled in the ground, and α the attenuation constant characteristic to the ground material. The order of magnitude of the maximum depth that the radar can explore is called the skin depth, defined as $\delta = 1/\alpha$. The Maxwell equations show that $\alpha \approx 0.0053\sqrt{\sigma_r}/\delta$(GeoSci Developer, 2017) where σ is the electric conductivity of the material and σ_r is the relative dielectric permittivity of the material.
Table 2 shows the electromagnetic properties of various rocks and material that can be found on Mars. Figure 1 shows the skin depths of various rocks according to the frequency of the electromagnetic waves.

This project has received funding from the European Union's Horizon 2020 research and innovation programme under MSCA-RISE2020 grant agreement No 101007973.

Table 2: Electromagnetic properties of natural materials.

Material	ϵ_r	σ (mS/m)
Air	1	0
Fresh Water	80	0.5
Sea Water	80	3000
Ice	3-4	0.01
Dry Sand	3-5	0.01
Saturated Sand	20-30	0.1-1
Limestone	4-8	0.5-2
Shales	5-15	1-100
Silts	5-30	1-100
Clays	5-40	2-1000
Granite	4-6	0.01-1
Anhydrites	3-4	0.01-1

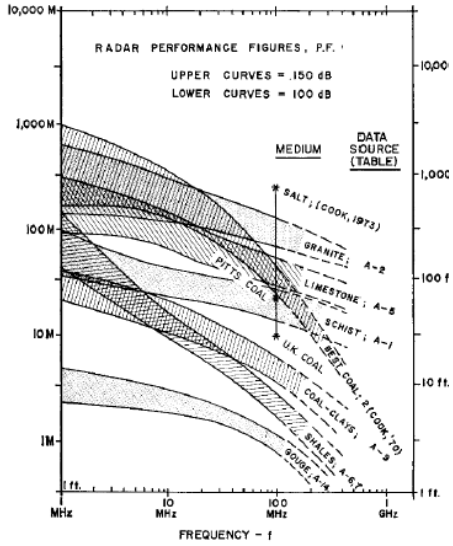

Figure 1: Radar probing distance (also called skin depth) according to the frequency of the electromagnetic wave and the considered rocks. For example, the skin depth for shales at 100MHz is around 5m.

4. Overview of the Martian environment

4.1. Geological description of the Martian upper crust

The possible range of the geological and environmental parameters of the top 40 m of the Martian crust and ice caps are listed in the Table 2. Although these different geological features could be thicker than this 40 m, however they are characterized in general below with specific focus on their top near surface part. These descriptions will form the basis for the Task 1.3 (Martian Surface and Subsurface Physical Parameters) and the Task 1.4 (Martian Surface and Subsurface Stratigraphic Parameters).

This project has received funding from the European Union's Horizon 2020 research and innovation programme under MSCA-RISE2020 grant agreement No 101007973.

Table 2: Overview of the Martian surface and subsurface geological features.

Name of feature	Characteristics	Occurrence on Mars	Expected radar relevance and numerical characteristics	Potential analogues on the Earth
permanent polar caps	layered ice-dust mixture, mainly of H_2O ice but CO_2 ice could be present as buried units too	northern and southern polar region, however less ice at mid-latitude region might be also present in buried form	variable reflection but usually strong, well defined reflectors with good possibility for stratigraphic analysis	polar caps and high mountain ice masses (not analysed in this project)
polar layered deposits	layered dust-ice mixture, mainly H_2O ice, with few CO_2 ice also (Castaldo et al. 2014)	north and south circumpolar regions, and also below the polar caps	variable reflection but usually strong, well defined reflectors with good possibility for stratigraphic analysis	few locations might be relevant, especially at high latitude or altitude regions with active ice deposition simultaneously with Aeolian dust transport
seasonal shallow subsurface hydration	modified according to seasons and climatic changes, influencing the H_2O content of the top few m layer	currently as annual seasonal cycle in the circumpolar region, on Ma long timescales could occur anywhere by climatic changes	might be present where high humidity is followed by long dry season without much vegetation and soil cover	analysis of desert area right after and also long after heavy rains
mid latitude buried ice layers (areally extended)	shallow subsurface snow structured H_2O (Dickson et al. 2015) blanketed with dm-m thin dust cover, occasionally several 10 (up to 100) m thick (Harisch et Lal. 2020) more compacted ice masses	above 45°-50° latitude on both hemispheres	strong reflectors at their boundaries	rare, occasionally at high latitude or altitude sites
rock glacier—like features with buried ice	buried massive ice bodies, probably creeped and moved under different climatic conditions, showing	middle and high latitude region inside depressions, both in isometric	strong reflectors at their bottom boundaries	glaciers and rock glaciers on the Earth

This project has received funding from the European Union's Horizon 2020 research and innovation programme under MSCA-RISE2020 grant agreement No 101007973.

(concentrated in depressions)	glacier and moraine like surface features	depressions (craters) and elongated valleys		
mass movement features	mass movement produced debris, including rock and icy layer fall (Fanara et al. 2016), slump (Tsifge et al. 2006), creep	at many locations, mostly regardless surface feature types	structural information on the moved material, inferred water content, original surface identification below	any terrain type where mass movements happens
various non-ice dominated deposits: fluvial sediments, crater lakebeds, large plains (Meridiani, southern circumpolar)	indicates method and cyclicity of transport, style of deposition, partly infers to paleo-environmental conditions, localization of astrobiology relevant targets, geological history	at channels' mouth, basins, next to steep walls	determine grain size, boulders, layering,	specific group of sediments, especially water related ones at desert areas
Aeolian dune features	current and past active features, might indicate cementation and atmospheric density related changes	mainly at the northern circumpolar erg, and southern crater interiors	internal porosity or ice content, layering, bedding style	dunes in desert areas
duricrust	top cemented part of the regolith where grains are connected by later formed sulphates and iron-oxides	could be present at possibly any locations in the top few cm part of the regolith	decreases internal porosity by mineral cementation, below a more porous underlying regolith, could have elevated OH content	cemented features on loose sand and dust at desert areas, including desert pavement or salt crust

4.2. Geophysical and geological characteristics of Mars

4.2.1 Deep Internal structure of Mars

The deep internal structure of Mars is inferred from chemical models and the behavior of the planet on its orbit, from which the moment of inertia can be derived. Combining both approaches, it is currently thought that the core of Mars, of radius 1700–1800 km, has a composition dominated by iron, with a sulfur content, 14–17%, higher than the Earth's sulfur content (e.g., Smrekar et al., 2019). More precise results should be

This project has received funding from the European Union's Horizon 2020 research and innovation programme under MSCA-RISE2020 grant agreement No 101007973.

obtained by the RISE radio experiment of the ongoing InSight mission, working with the DSN tracking stations on Earth, then similarly, by the LaRa radio experiment onboard the ESA/Roscosmos ExoMars2022 lander. Whether the core is liquid, at least in part, is not yet established; however, strong magnetic anomalies measured in the southern highlands, from data collected by the MAG-ER instrument of Mars Global Surveyor and the MAG instrument of MAVEN, point to the existence of a dynamo that was active in the earliest stages of planetary evolution (e.g., Langlais et al., 2019).

The composition of the mantle is similar to those of the Earth's mantle, extends to a depth constrained by gravity and topography, the inversion of which can be used to infer the thickness of the crust and its variations. The depth of this interface is especially sensitive to magmatic crustal accretional processes, which are influenced by the acceleration of gravity through magma source rock adiabatic melting (Mège and Masson, 1996). Since Mars is smaller both in size and mass than the Earth, acceleration of gravity at the surface is lower, 3.7 m/s^2, three times less than on Earth, resulting in much more melt when thermal plumes rise from the mantle, This makes possible heavier crustal loads, and deeper crust-mantle boundary, once equilibrated by isostasy or flexure. It may also be influenced by the topographic dichotomy boundary (e.g., Andrews-Hanna et al., 2008). The true depth of the crust-mantle boundary, in lack of geophysical prospecting conducted at surface, is however relying in large part on the way gravity and topography are related, resulting in contrasted models suggesting to vary between 1 and 100 km, or more (e.g., Andrews-Hanna et al., 2008; Goossens et al., 2017).

Crustal magnetization may be related to ancient global magnetic field during crust formation, and also related to fluids especially related to the very active hydrological system of Mars during the Noachian, which may have incorporated huge amounts of water into the crust (Carr and Head, 2015). Water may have been stored in serpentine, which would explain the formation of magnetite that recorded the magnetic field at that time (Chassefière et al., 2016), and if released by deserpentinization, could make a deep water reservoir, part of which should be still present nowadays.

New water crustal reservoirs may have formed during the Hesperian and Amazonian, but at shallower depth; Carr and Head (2019) estimate that 20–30 m of global equivalent layer of water still exists in the Martian crust today but in other format. This shallow level is possibly stored as groundwater in its deeper part, and as ground ice (cryosphere) in its upper part, the depth of which is largely dependent on latitude (Clifford et al., 2010). The latter, or its uppermost portion, is potentially detected by radar sounding, hence by a FlyRadar system.

At the shallowest level, information provided by radar sounding is ideally completed by data provided by gamma ray and neutron counters. These instruments detect hydrogen in the surface based collision with cosmic rays in the first 1 m below the surface. HEND is a neutron counter that operated on the Mars Odyssey orbiter, whereas GRS was counting gamma rays. FREND, a version of HEND that has higher resolution, is currently operating on ExoMars Trace Gas Orbiter. These instruments have been used for global hydrogen emission mapping. Similar instruments can be used on the ground. Two versions of ADRON will operate on the ExoMars2022, on the lander and the rover. The subsurface H_2O content influences the radar signal thus important for this project.

4.2.2. Martian radar sounding systems on Mars: an overview

Space-borne radar systems used to observe planetary surfaces and subsurfaces, can be divided into two categories: imaging radar (Synthetic-Aperture Radar) and sounding radar. SAR images are generally used in remote sensing and mapping the surface of the Earth and other planets (e.g. the surface of Venus). Sound-

This project has received funding from the European Union's Horizon 2020 research and innovation programme under MSCA-RISE2020 grant agreement No 101007973.

ing radar was used to study the surface of Mars in two missions: Mars Express and Mars Reconnaissance Orbiter, for probing the subsurface and in particular, to search for ice and water layers in the polar caps and the cryosphere. MARSIS and SHARAD have evidently demonstrated the efficiency of the radar sounding approach in planetary remote sensing.

The main use of radar sounding in geology is to capture echoes from the subsurface in the nadir direction. The output is a two-dimensional image called "radargram" that represents the dimensions of azimuth (along-track) and range (time-delay, a function of depth). Such profiles can be compared with geologic cross-sections, once clutter is identified and removed from the signal. Radargram processing for geological interpretation presents similarities to the processing required to interpret seismic cross sections. Surface echoes are also used to derive the dielectric constant (permittivity) of the near-subsurface. Dielectric constant is a physical property of materials especially useful in geology to determine the rock composition, porosity, and ice or liquid water abundance (Grima et al., 2012; Mouginot at al, 2010; Orosei at al., 2018).

Sounding radar wavelengths are usually in the range of several meters (frequency of 50 – 100 MHz) to >100 m (frequency of <3 MHz). Radargrams obtained from such radars make it possible to identify features to a depth of 10s-1000s meters below the surface (the highest values are obtained in polar caps, Plaut, 2020).

	SHARAD	MARSIS
Frequency band	15–25 MHz chirp	1.3–2.3 MHz, 2.5–3.5 MHz, 3.5–4.5 MHz, 4.5–5.5 MHz chirps
Vertical resolution, theoretical, reciprocal bandwidth, $\varepsilon_r = 4$	7.5 m	75 m
Transmitter power	10 W	10 W
Pulse length	85 μs	250 or 30 μs
PRF	700/350 Hz	127 Hz
Antenna	10-m tip-to-tip dipole	40-m tip-to-tip dipole
Postprocessor SNR (worst-best)	50–58[a] dB	30–50[b] dB
Horizontal resolution (along track × cross track)	0.3–1 km × 3–6 km	5–10 km × 10–30 km

[a]Estimate.
[b]Actual.

Table 3. SHARAD and MARSIS instrument parameters (Seu et al., 2007)

MARSIS (Mars Advanced Radar for Subsurface and Ionospheric Sounding) was designed to explore the subsurface and ionosphere of Mars. The radar acquires data from altitudes lower than 1200 km. The radar is a dual channel low-frequency sounder that operates between 1.3 and 5.5MHz for subsurface sounding, and between 0.1 and 5.5MHz, for ionospheric sounding. All periods of operation when the spacecraft is below 900 km altitude are considered data acquisition opportunities for the MARSIS subsurface sounding mode, while the periods when the spacecraft is between 900 and 1200 km in altitude are allocated to ionosphere sounding operations (Jordan et al., 2009).

MARSIS was also intended to investigate and study ionospheric properties, which could affect the subsurface signals. Ionospheric measurements showed structures (Gurnett et al, 2005) that are related to the remnant crustal magnetic field (Langlais et al., 2019).

SHARAD (the SHAllow RADar) uses a 15 to 25 MHz frequency band, resulting in shallower penetration but higher resolution than MARSIS (Table 3). The horizontal resolution of SHARAD is between 0.3 and 3 kilome-

This project has received funding from the European Union's Horizon 2020 research and innovation programme under MSCA-RISE2020 grant agreement No 101007973.

ters and a vertical resolution is about 15 meters in free space, which corresponds to a depth of more than 10 meters in the Martian subsurface.

RIMFAX (Radar Imager for Mars' subsurface experiment), the ground-penetrating radar (GPR) located on the Perseverance rover of Mars2020 at its landing site, can reveal subsurface structure and its composition to 10 m depth, including the presence of water ice, buried sand dunes or lava features. Using a bow-tie slot antenna, RIMFAX operates at 150-1200 MHz radio frequencies (Hamran et al., 2020).

WISDOM (Water Ice and Subsurface Deposit Observation on Mars) is another GPR radar, designed for the Rosalind Franklin rover of the ExoMars2022 mission and help to understand the geologic and hydrologic context of potential biosignatures and biomarkers. This radar will operate in the 0.5-3 GHz frequency range, providing imaging to a depth of 3 meters (Ciarletti et al., 2017).

4.2.3. Global mapping of surface reflectivity

Mouginot et al., 2010 presented a 3–5 MHz global reflectivity map of mars from MARSIS (fig. 2). The reflected signal is composed of coherent and incoherent reflections, which inform us on the electric properties and roughness of surface, respectively. The total volume of ground ice stored at the poles at depth down to 60-80 m is found to be on the order of 10^6 km^3, whereas the Martian atmosphere contains an additional 3 km^3 of condensed water residues (Plaut et al., 2007).

With a dielectric constant of 3.1 for pure ice (Petrenko and Whitworth, 1999), and 6-11 for volcanic rocks (Campbell and Ulrichs, 1969), the proportion of ice versus rock could be determined if the porosity is known. The obtained ice and rock volume mixing ratios were found to be about 50% on average in the south, and 50-100% in the north (Mouginot et al., 2010).

Global dielectric constant mapping of Mars was also done using the SHARAD data, complementing the results obtained by MARSIS (Castaldo et al., 2017). Similarly, though at shallower depth (< 15 m), it was found that the dielectric constant in the southern hemisphere (6 to 10+) is on average higher than in the northern hemisphere.

Radar relevant characteristics of the Martian geological features

The main features of the Martian surface and shallow subsurface, interesting for GPR studies are summarized in the Table 1, their further descriptions are presented below, classified to the main topics widely used in the literature. To see the potential capabilities of a GPR-SAR applying for Mars, requires a survey on the occurrence and characteristics of different layers, compositional plus structural variability, and discontinuities there, which are mainly connected to volcanic and sedimentary emplaced structures presented after a theoretical based general overview below.

Several differences of radar properties are expected to occur on Mars compared to those on the Earth, based only on theoretical argumentation. The gravity driven pore compaction depth is larger on Mars but this will not influence shallow radar analysis. The average temperature of target rocks is lower compared with Earth but does not influence much the radar response, however might be considered in specific cases (Stillman and Olhoeft 2006 and 2008). The pore gas pressure is lower but does not influence radar reflectance, however unfilled **porosity might be more abundant on Mars**, because subsurface fluids considered to be less abundant on Mars, thus pore filling by mineral cementation or condensation could be less frequent there. **Salty brines** might exist in the subsurface of Mars with probably much higher salt content than on the Earth. The surface is generally more oxidized than most areas on the Earth what

This project has received funding from the European Union's Horizon 2020 research and innovation programme under MSCA-RISE2020 grant agreement No 101007973.

influences the mineral composition and oxidization of minerals there, but only at cm or m thickness. The target rocks might be less hydrated in the upper subsurface while in the deeper subsurface **hydration and bulk ice content** could be more abundant than on Earth. Subsurface carbon dioxide ice might be present at unique polar locations, which has consequence on radar reflectance, difference relatively to water ice might be also considered. Wide range of solid H_2O states and structures is expected including snow, firn and bulk ice in the subsurface, what although exist on the Earth too, however rarely analyzed by GPR methods. The shallow subsurface ice masses exists at much wider areal occurrence than on Earth, and the dust content of this snow / ice masses could be larger and more variable, as well as more structured (layered) than on the Earth.

During the analysis of Mars, dielectric contrast is searched for in the subsurface and identification of reflectors' stratigraphy helps to reconstruct subsurface continuity or discontinuity of layers, faults, folds etc. as various contrasts, especially between dust and ice (Nunes and Phillips 2006). Dielectric properties are influenced by small grain size material like clays (Colantuono et al. 2014) on the penetration depth of radar signal, what might be also influenced by water content, somewhat the temperature and electric properties of the minerals. The GPR-SAR method allows the identification of buried impact craters and other subsurface features. During the evaluation of reflectors these structures might be assumed to be isochronous layers if geological context support this situation, however different thickness of the same units might exist at different locations. The GRP measured dielectric contrast could be caused by different material and grain size deposits, also could arise form facies, porosity and fluids related variations.

4.2.4. Ice deposits

The large ice caps at the poles with the Polar Layered Deposits (PLD) below them are the largest recognized water reservoirs on Mars (Bibring, J.P., 2004). In both **polar caps** extensive subsurface layering is abundant, where layer packages could be identified with thickness of 10-100 m, porosities could be >40% at the surface that decreases with depth into a zero-porosity at about <0.5 m – however heterogeneity seems to exist. In the Northern Polar Cap the average dielectric constant is 3.10 (σ = 0.12) and a loss tangent <0.0026 (σ = 0.0005), probably has volume of ice is pure at ≥95% (Grima et al. 2009). The residual cap in the North is mostly made up of pure water ice (Grima et al., 2009), is approximately 1450 km in diameter and 3 km thick (Figure 2), Unconformities, erosional surfaces could be observed many locations. Beside the manly H_2O ice structure, CO_2 ice could be also present at depth, for example at 320 m in the northern polar cap (Smith et al. 2016) in the last 0.37 Ma. The southern residual polar cap is also layered, have a smaller diameter (355 km), but its greater thickness makes the volume of ice on both sides of the globe comparable. The relative volume of the polar caps vary small with seasons, following an accumulation-sublimation cycle – their most volume was accumulated during different climatic periods. At Planum Australe low reflectivity pure CO_2 ice exists in three layers correspond to episodes of atmospheric collapse in the last 370,000 years, each capped by a ~30-m layer of water ice to prevent sublimation (Bierson, et al. 2016).

Polar layered deposits also show extensive almost horizontal layering with many interesting specific aspects: SHARAD radar already observed disconformities in the upper 500 m of the NPLD, representing during 4. Ma, however beside the erosional unconformities, which are abundant, deformation due to flow is sparse. Beside the characteristic dust and H_2O ice components, subsurface CO_2 ice was identified in the southern PLD (Phillips et al 2010) in the form of ~5 m of solid CO_2 underlain by an apparently thin layer of

This project has received funding from the European Union's Horizon 2020 research and innovation programme under MSCA-RISE2020 grant agreement No 101007973.

water ice, permittivity was found to be ϵ' = 2.0-2.1, with a σ of 0.2. Analyzing the southern polar layered deposits in general measured values presented relative dielectric constant of 3.0–5.0, conductivity 1.0–2.0 × 10–6 S/m, and the relative dielectric constant of the basal layer is 7.5–8.5 with conductivity around 1.0 × 10–7 S/m. These indicate dust content varying from 0 to more than 75% (Zhang et al. 208). The characteristics of the surface and subsurface echoes over most of the SPLD signifies a composition of water ice that is overlying a typical Martian regolith and crust. Observation of the surface of the SPLD indicates a lag of dust or rocky material that is clearly thin at MARSIS wavelengths, indicating that it is a deposit no more than a few tens of meters thick (Plaut et al., 2007).

The MARSIS data show strong basal echoes in the south part of the SPLD that have been interpreted as an effect of the presence of liquid water below the SPLD at depths about 1.5 km. This feature has been interpreted as a buried steady body of liquid water. Before this discovery, liquid water had already been suggested in the northern plains at the Phoenix landing site, where concentrations of substantial amounts of magnesium, calcium and sodium perchlorate in the soil had been found (Hecht et al., 2009).

In addition to finding the structure and composition of ice at the polar caps, radar sounding data have been used to identify ice-rock mixtures at depth in other non-polar regions. For instance, interpretation of SHARAD data revealed the presence of an icy regolith in the northern lowlands in Utopia Planitia (UP), where a variety of glacial or periglacial landforms have been documented. The ice-rich level extends to a depth of at least 80-170 m, covering a surface area of 375 000 km^2 (Stuurman et al., 2016).

Large number of **glacier and rock glacier features** are present on Mars, which were classified based mostly on their surface structure to lobate debris apron (LDA), lineated valley fills (LVF), and concentric crater fills (CCF): LDA and LVF reveal low radar loss and basal reflectors with high power that imply nearly pure glacial ice throughout most of their depth (Baker at al. 2018). The basal contacts between the glacier ice and underlying bedrock could be often resolved. Inside them water ice is present with <20% lithic debris, dielectric constant for the surface rocky debris is 4.9 ± 0.3 in the cases observed by Petersen et al. (2017). Assuming basalt rock, this value is consistent with a porous debris containing up to 64% ice, or an ice-free debris layer with porosity of 28-34%. Many LVF, and LDA have low loss tangents consistent with ice content (Campbell et al. 2018). At icy terrains erosion/accumulation periods might happen in the past, what left behind dry lag deposits and ice masses, in sandwich like layered structure. The existence of the former ice accumulation or sublimation and erosion dominated periods could be inferred from GPR data in the form of different ice containing and different porosity/density layers. Lobate Debris Aprons (LDA) are viscous flow features having thickness of hundreds of meters and width typically 10 km that extend from high relief slopes (Carr et al., 1977). These features are associated with lineated valley fill and concentric crater fill and are thought to be remnants of glacial ice from an earlier climatic regime. SHARAD data suggest that the LDA found in Deuteronilus Mensae on the northern edge of Arabia Terra are composed mostly of water ice (Plaut et al., 2009).

Ice-filled craters and valleys have also been documented in the northern hemisphere and investigated using MARSIS or SHARAD, such as Korolev and Dokka. Korolev crater is 3.1 km deep and 82.83 km in diameter. Dokka, closer to the North Polar Cap, is slightly smaller, 2.5 km deep and 51.26 km in diameter (Conway et al., 2012). In these craters, the dielectric constant may be locally as high as 11–12, denoting a dominantly rocky content, but is generally also very low (<5), consistent with geomorphological indications of very high ice content, or even pure ice (Castaldo et al., 2017). Data from TES, THEMIS and CRISM confirm that water–ice or a dominantly water–ice rich formation occupies the interior of Korolev (Armstrong et al., 2015).

This project has received funding from the European Union's Horizon 2020 research and innovation programme under MSCA-RISE2020 grant agreement No 101007973.

The idea that an ocean once covered the northern hemisphere north of the dichotomy boundary, was proposed by Clifford and Parker (2001) based on the interpretation of possible shorelines from geomorphology and is still controversial. The dielectric constant contrast found from MARSIS (Mouginot et al., 2010) and SHARAD (Castaldo et al., 2017) data was interpreted as a supplementary clue to the existence of such an ocean in the past (Mouginot et al., 2012).

Figure 2. North Polar Cap radargrams and orbit track by SHARAD and Marsis (Plaut, 2020). Note that the top some 10 m layers are unresolved by the already worked radars at Mars.

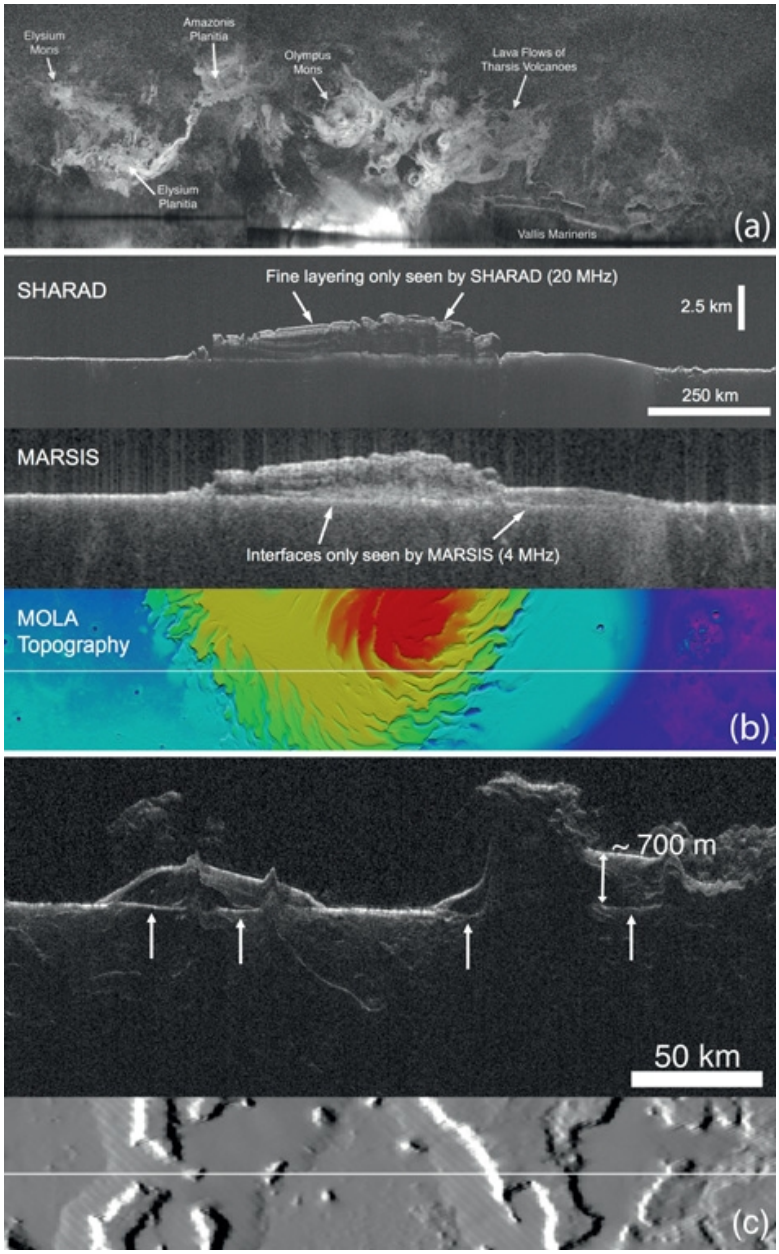

This project has received funding from the European Union's Horizon 2020 research and innovation programme under MSCA-RISE2020 grant agreement No 101007973.

4.2.5. Volcanic structures and volcanic deposits

Volcanic activity on Mars is thought to be more easily explosive than on Earth due to the lower gravity (Wilson and Head, 1994) and the lower atmospheric pressure, increasing the bubble formation in the ascending magma. As a consequence, the quantity of porous rocks resulting from airfall deposits is thought to be proportionally higher than on Earth, what could be qualified with GPR according to their porous voids. Similarly, vesicularity is thought to be more frequent in lava flows. Because the dielectric constant of air is 1, such porous rocks are detected by MARSIS and SHARAD as low dielectric constant regions, where rock porosity is an alternative to the presence of ice. For these reasons, many works have focused on the interpretation of MARSIS and SHARAD data in volcanic regions. The Tharsis region, a volcanic plateau on Mars, is dominated by three shield volcanoes: Ascraeus Mons, Pavonis Mons and Arsia Mons. Measurements from SHARAD showed buried lava flows in this area. Arsia Mons is morphologically unique; it is the most developed volcano with a large diameter caldera relative to the host shield. On the northwestern flank of AM discovered the remnant of glaciers from the late Amazonian period (Head and Weiss, 2014). In multiple locations, SHARAD data in the Arsia Mons caldera show reflections (Figure 3) suggesting the presence of possible vesiculated lava flows on the top of denser lava flows. Another possibility is the presence of a thick layer of pyroclastic materials between thin lava flows (Ganesh et al., 2020).

Volcanic units were surveyed on the planet, where discontinuity at layers from lava flows and differences in porosity (especially from low porosity tuffs) are expected to show strong radar response. Already analysed targets in the Elysium-Utopia region showed at the basaltic plain permittivity of 2.6 ± 0.9 suggesting subsurface water ice or a layer of dry and low-density deposits beneath the basalt layer around 40 m depth (Nunes et al. 2010) by SHARAD data. Interfaces of basaltic flows have been observed at several locations around the Tharsis Provence (Shoemaker et al. 2012). The possibility of lava cave detection was presented at Alba Mons (Perry et al 2019), however no firm confirmation was achieved yet. In Vastitas Borealis volcanic plain area at lava ridges subsurface dielectric horizon follows the surface topography, indicating emplaced prior to compressional tectonic deformation (Campbell et al. 2008).

Pyroclastic deposits may extend far from their eruption center, and Medusae Fossae is an example where such deposits may have been found. Data from the Mars Global Surveyor mission suggest the occurrence of buried channels in several regions in the Medusae Fossae Formation, located between the Tharsis and Elysium volcanic centers. The material seems to be a friable as well as irregularly consolidated airfall volcanic deposit (Bradley et al., 2002). MARSIS data on the Medusae Fossae Formation (Figure 4) show deep reflectors at a depth of about 2 km (Plaut, 2020). The dielectric constant is near 3, consistent with a low-density or even high-porosity lithic deposit (ash or dust), perhaps also including ice (Watters et al., 2007).

This project has received funding from the European Union's Horizon 2020 research and innovation programme under MSCA-RISE2020 grant agreement No 101007973.

Figure 3. Orbit tracks (white line, left) and SHARAD radargrams (right) in the caldera of Arsia Mons (Ganesh et al., 2020). The colored symbols are geologic features observed on radargrams (see Ganesh et al. 2020 for details).

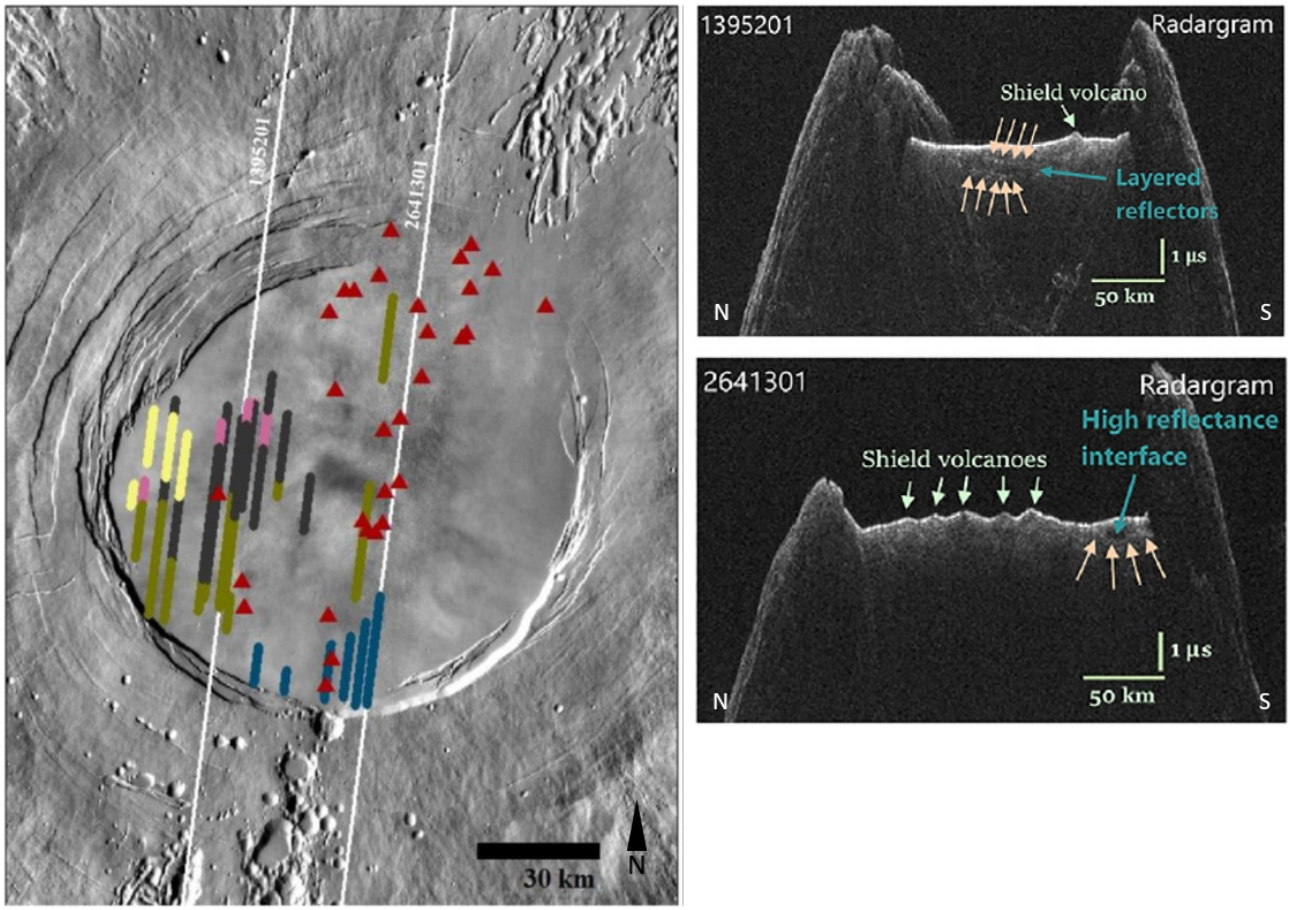

This project has received funding from the European Union's Horizon 2020 research and innovation programme under MSCA-RISE2020 grant agreement No 101007973.

Figure 4. MARSIS radargram and orbit 4117 track showing MFF deposit (Watters et al., 2017).

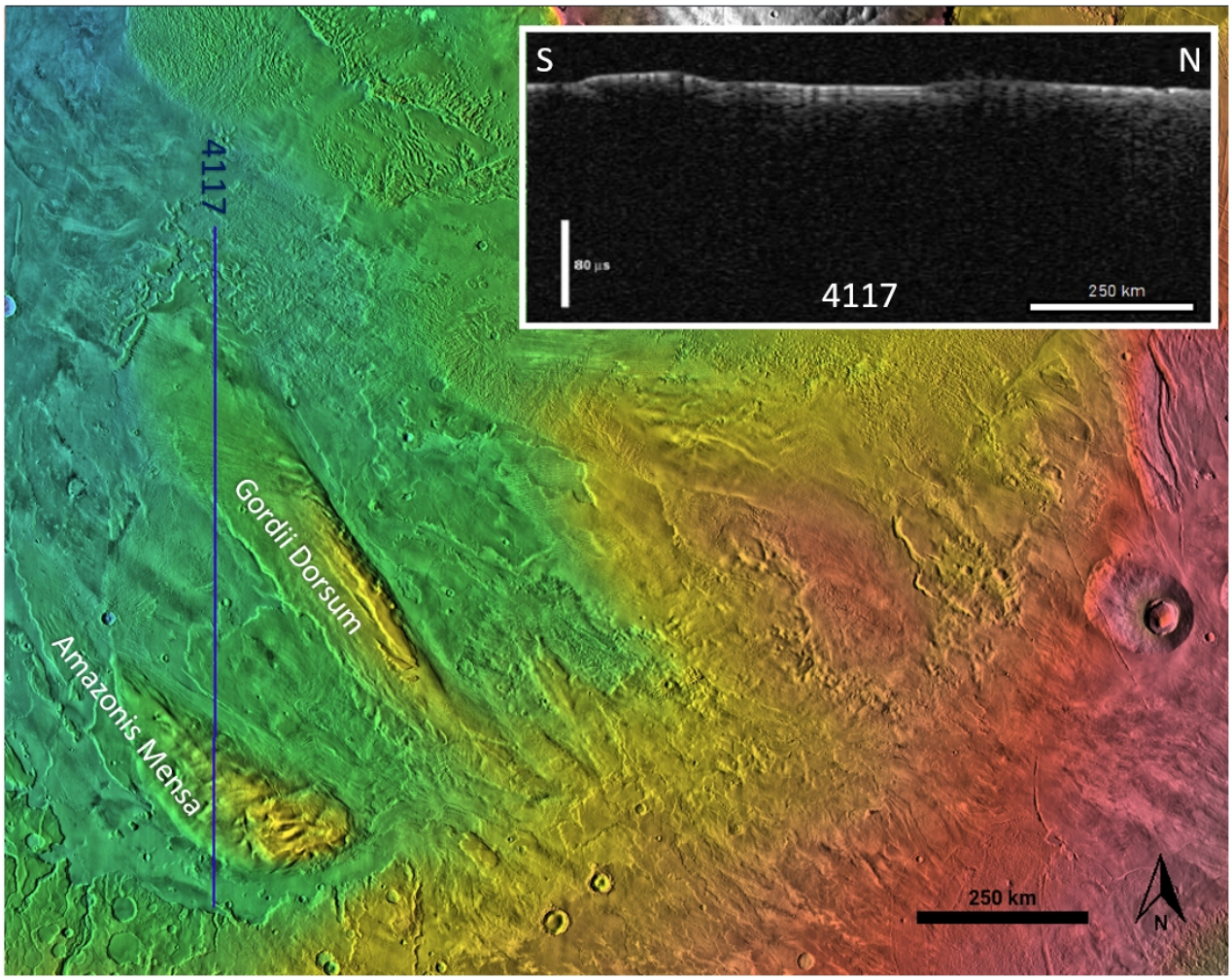

Craters might show subsurface discontinuities at the bottom of their ejecta blanket or intra-crater back fallen debris, or in the case of subsurface circulating fluids generated mineral cementation inside faults. In the case of buried craters, they could be identified by radar, like in the case of large impact craters at the northern lowland found by MARSIS (Watters et al. 2006). In pedestal craters (Nunes et al. 2009) the material in the ejecta blanket often showed bulk permittivity of 4.5 to 5.0 ad being radar-transparent, and observations were consistent with either a porous basaltic matrix or a mix of basaltic material and water ice.

Sediments are usually accumulated in lows and if not buried could be ideal target if shallow subsurface radar analysis. An important aspect of the Martian sediments' radar properties is their possible H_2O content, mainly in the form of ice. The wind erosion influenced, low density material composed **Medusa Fossae Formation's** (MFF) lower layers might contain ice (Campbell et al. 2021). The central plain called Lucus Planum (Caprell et al. 2016) composed of pyroclastic flows or airfall and ice, where SHARAD revealed 97 reflectors. The dielectric constant in the eastern and SW sectors were 2.3 by highly porous material,

This project has received funding from the European Union's Horizon 2020 research and innovation programme under MSCA-RISE2020 grant agreement No 101007973.

while in the NW sector was 4.5, implying the presence of denser materials. The detected subsurface reflector of low permittivity (nearby water-ice) bearing materials was observed along the rise of south terrain (10.12° N, 220.10° S) towards roughest surface of MFF southwest of Olympus Mons" (Anul et al. 2018). The Hesperian aged **Dorsa Argentea Formation** (DAF) was once ice rich and may still contain ice, and both SHARAD and MARSIS based loss tangent values indicate dry sediment but a fraction of remnant ice at depth may occur (Whitten et al. 2020).

Plain units also show a range of radar features, including subsurface layering, lava flow-features and occurrence of water ice. The main aims during the survey of plains could be the identification of buried ice occurrence, probable atmospheric effect related hydration, and former weathering surfaces. Extensive subsurface reflector was found in Arcadia Planitia (180-225E, 38-50N, Bramson et al. 2014) by jointly evaluating several datasets, by the constrains on the dielectric constant indicate this decameters-thick layer seems to be relatively pure excess ice. At Athabasca Valles on the Cerberus Plain (Alberti et al. 2012), in the area of the hypothesized frozen sea, mixture of volcanic rocks with either ice or air in porous voids was identified by the SHARAD instrument.

Fluvial features are also important target of a high resolution shallow subsurface radar, if information on their material's grain size could be made. Identifying different sized, shaped and stratigraphic location fluvial sediments infer to flow regime, discharge, flowing speed, while possibly cyclicity could be also present. Fusing these with other data types, results infer to past climatic conditions. For example, Hebrus Valles (Nerozzi et al. 2020) and Hephaestus Fossae as Early Amazonian aged outflow channels were analysed by subsurface mapping, indicating volcanic layers and ice bearing composition too. Central Elysium Planitia with volcanic and subsurface fluvial signatures showed radar reflectors with possible connections between the plain and outflow channels, such as Athabasca Valles and Marte Vallis (Xiong et al. 2021). The original fluvial eroded bed of Marte Vallis was also identified by SHARAD, which formed prior to burial by younger lava flows (Morgan et al. 2011). However, it can be stated that few results have been gained on the fluvial regime related to sedimentary aspects, probably because of the SHARAD and especially MARSIS are optimized to identify larger structures than expected at fluvial deposits. The same is relevant for open lake basins, where few ancient wet sedimentation features have been identified by radar yet (Shoemaker et al. 2018).

Dunes on Mars are relatively thin features thus difficult to analyze in details by SHARAD and MARSIS, partly because in cases the radar signal scattering by wavelength-scale dunes often prevents detection of subsurface features (Putzig and Hoover 2018). Thus many dunes severely scatter radar signals were present, while others allow them to penetrate, presenting internal layering and underlying surfaces, some of which are related to subsurface ice (Putzig 2017) for example in Lowell crater or Ganges Chasma. Future shallow subsurface focused high resolution radar survey are expected to reveal a wide variety of depositional features inside dunes and related climatic signatures. Dunes at cases are expected to be formed by interbedded ice layers, what could be identified by radar.

Regolith: the weathered and usually loose (although somewhere partly cemented) part of the shallow subsurface, influenced by various external forces, and produced from the original bedrock below. While the fragmented lower part of the regolith also called megaregolith could be km thick, in this work the shallow, top 100 m thick regolith layer is considered, keeping in mind the global variability the thickness the regolith (regardless its definition) changes. The topmost layer is also called Martian soil, although there is no observation on possible biological effect in it opposite to the soil term used on the Earth. The Martian regolith is probably a complex lithological unit, the topmost loose part is composed of dust and larger

This project has received funding from the European Union's Horizon 2020 research and innovation programme under MSCA-RISE2020 grant agreement No 101007973.

grains including cm, dm and m sized rock blocks, where the finer grains at sites are cemented by sulfates and iron-oxides plus –hydroxides. This top few cm thin straightened layer is also called duricrust. From the GPR analysis point of view vertical changes are expected by the coarsening of grain size downward, decreasing oxidized (reddish) state and getting poor communication with the atmosphere (volatile exchange) toward the deeper regions. The surface exposing UV radiation mainly changes the chemical structure in the top some mm layer, the ionized particle irradiation has partly similar effect on the top 1-2 m thick layer. From the atmosphere H_2O could condense / freeze to the top of the regolith with changing the porosity, composition and hydration state. The regolith could be modified by wind (only its very thin top layer), hydration/dehydration, or rarely by impacts.

6 Conclusion

The subsurface of Mars clearly shows rocky and icy levels of variable composition from altered levels and sediments to fresh volcanic rocks and ices. The 3D geometry of these levels in the shallow subsurface remains generally unknown while based on the outcrop walls a wide range of potentially observable features exists in the top 100 m of the regolith, and they are valuable indicators to understand Mars and its evolution. The GPR technique has already been applied to Mars with good results since two GPRs installed on orbital platforms have already produced results allowing major scientific advances, demonstrating that useful data on dielectric constant, permittivity, porosity, reflector depths could be gained, however have not been acquired for the shallow subsurface region, what would support next missions. GPRs permit to image the subsurface of such a planet down to 100 m in good conditions that lack liquid water or high concentration of metals.

As ice is more abundant in the shallow subsurface than the surface of Mars, thus good chance exists to identify subsurface ice units. Porosity could be more often left intact (unfilled voids) on Mars than on Earth because of less subsurface fluid migration and slow weathering processes, providing a larger variability in subsurface echoes and wider possibility to infer target characteristics, as original porosity could be indicative of various aspects. Shallow subsurface might be more recently formed than deeper subsurface in general, thus a radar with >100 m penetration surveys layers relevant to recent climatic changes related modifications, including ice occurrence and hydration. Shallow subsurface region is relevant for ISRU activities thus could be closely liked to Mars Sample Return and later human missions. Separation of ice and pore voids in radar data requires focused methodological development

The data presented in this report specify the interest of GPR for the analysis of the Martian subsurface. The general dryness, together with the poor weathering state of the regolith compared with those on the Earth, the expected good preservation of original porosity, wide range of potential discontinuities, and the spatially concentrated occurrence of clay sized grains together make the Martian regolith as a target with variable conditions observable to a GPR there. These data will be re-used in later phases of the project to define the characteristics of the demonstrator and to identify regions of the Earth with characteristics similar to the Martian regions of interest. The instrument that will be developed in the frame of FlyRadar project, will be tested at one or more of these analogous regions.

This project has received funding from the European Union's Horizon 2020 research and innovation programme under MSCA-RISE2020 grant agreement No 101007973.

4.2.6. Bibliography

Alberti, Giovanni; Castaldo, Luigi; Orosei, Roberto; Frigeri, Alessandro; Cirillo, Giuseppe 2012. Permittivity estimation over Mars by using SHARAD data: The Cerberus Palus area. Journal of Geophysical Research, Volume 117, Issue E9, CiteID E09008.

Andrews-Hanna, J.C., Zuber, M.T., and Banerdt, W.B., 2008. The Borealis basin and the origin of the Martian crustal dichotomy. Nature 453, doi:10.1038/nature07011.

Anul Haq, Mohd; Ansari, Shahid Iqbal 2018. Equatorial subsurface ice detection in the plains of southwest of Olympus Mons, Mars. 42nd COSPAR Scientific Assembly. Held 14-22 July 2018, in Pasadena, California, USA, Abstract id. B4.1-40-18.

Armstrong, J.C., Titus, T.N., Kieffer, H.H., 2005. Evidence for subsurface water ice in Korolev crater, Mars. Icarus 174, 360–372.

Baker, D. M. H.; Carter, L. M.; Morgan, G. A. 2018. Insight into the Subsurface Structure of Mid-Latitude Glaciers and Mantles on Mars from Impact Craters and Radar Sounding. American Geophysical Union, Fall Meeting 2018, abstract #P24D-09.

Bibring, J.-P., Langevin, Y., Poulet, F., Gendrin, A., Gondet, B., Berthé, M., Soufflot, A., Drossart, P., Combes, M., Bellucci, G., Moroz, V., Mangold, N., Schmitt, B., Omega Team, the; Erard, S., Forni, O., Manaud, N., Poulleau, G., Encrenaz, T., Fouchet, T., Melchiorri, R., Altieri, F., Formisano, V., Bonello, G., Fonti, S., Capaccioni, F., Cerroni, P., Coradini, A., Kottsov, V., et al. 2004. Perennial Water Ice Identified in the South Polar Cap of Mars. Nature. 428 (6983): 627–630.

Bierson CJ, et al. Stratigraphy and Evolution of the Buried CO2 Deposit in the Martian South Polar Cap. Geophysical Research Letters. 2016;(43)

Bradley, B. A., Sakimoto, S. E. H., 2002. Medusae Fossae Formation: New perspectives from Mars Global Surveyor. Journal of geophysical research, vol. 107, no. E8, 5058, 10.1029/2001JE001537.

Bramson, Ali M.; Byrne, Shane; Putzig, Nathaniel E.; Mattson, Sarah; Plaut, Jeffrey J.; Holt, John W. 2014. Distribution and Compositional Constraints on Subsurface Ice in Arcadia Planitia, Mars. American Astronomical Society, DPS meeting #46, id.203.05.

Bramson, A. M.; Byrne, S.; Putzig, N. E.; Plaut, J. J.; Mattson, S.; Holt, J. W. 2013. Thick subsurface water ice in Arcadia Planitia, Mars. American Geophysical Union, Fall Meeting 2013, abstract id.P43D-05

Campbell, Bruce A.; Morgan, Gareth A. 2018. Ice Content in Nonpolar Material from Multiband SHARAD Data Processing. Geophysical Research Letters, Volume 45, Issue 4, pp. 1759-1766.

Campbell, Bruce A.; Watters, Thomas R.; Morgan, Gareth A. 2021. Dielectric Properties of the Medusae Fossae Formation and Implications for Ice Content. Journal of Geophysical Research: Planets, Volume 126, Issue 3, article id. e06601

Campbell, Bruce; Carter, Lynn; Phillips, Roger; Plaut, Jeffrey; Putzig, Nathaniel; Safaeinili, Ali; Seu, Roberto; Biccari, Daniela; Egan, Anthony; Orosei, Roberto 2008. SHARAD radar sounding of the Vastitas Borealis Formation in Amazonis Planitia. Journal of Geophysical Research, Volume 113, Issue E12, Cite ID E12010.

This project has received funding from the European Union's Horizon 2020 research and innovation programme under MSCA-RISE2020 grant agreement No 101007973.

Campbell, M.J., Ulrichs, J., 1969. Electrical properties of rocks and their significance for lunar radar observations. J. Geophys. Res. 74, 5867–5881.

Caprarelli, G.; Orosei, R.; Rossi, A. P.; Cantini, F.; Carter, L. M.; Papiano, I.; Cartacci, M.; Cicchetti, A.; Noschese, R. 2016. Interpretation of Radar Sounder MARSIS Data from Lucus Planum, Mars: A Complex Geological Setting. American Geophysical Union, Fall General Assembly 2016, abstract id. P51C-2155

Carr, M. H., Schaber, G. G., 1977. Martian permafrost features, J. Geophys. Res., 82, 4039–4054.

Carr, M.H., and Head, J. W., 2015. Martian source/near surface water inventory: sources, sinks, and changes with time. Geophysical Research Letters 42, 726–732, doi:10.1002/2014GL062464.

Carr, M.H., and Head, J. W., 2019. MArs: Formation and fate of a frozen Hesperian ocean. Icarus 319, 433–443.

Castaldo, L.; Mège, D.; Orosei, R.; Séjourné, A. 2014. Buried CO2 Ice traces in South Polar Layered Deposits of Mars detected by radar sounder. American Geophysical Union, Fall Meeting 2014, abstract id. C21C-0359.

Castaldo, L., Mège, D., Gurgurewicz, J., Orosei, R., Alberti, G., 2017. Global permittivity of the Martian surface from SHARAD. Earth and Planetary Science Letters 462, 55–65.

Chassefière, E., Lasue, J., Langlais, B., and Quesnel, Y., 2016. Early Mars serpentinization-derived CH4 reservoirs, H2-induced warming and paleopressure evolution. Meteoritics and Planetary Science 51, 2234–2246.

Christensen, P.R., Bandfield, J.L., Bell, J. F., Gorelick, N., Hamilton, V. E., Ivanov, A., Jakosky, B. M., Kieffer, H. H., Lane, M. D., Malin, M. C., McConnochie, T., McEwen, A. S., McSween, H. Y., Mehall, G. L., Moerch, J. E., Nealson, K. H., Rice Jr, J. W., Richardson, M. I., Ruff, S. W., Smith, M. D., Titus, T. N., Wyatt, M. B., 2003. Morphology and Composition of the Surface of Mars: Mars Odyssey THEMIS Results. Science 300, 2056–2061.

Ciarletti, V., Clifford, S., Plettemeier, D., Le Gall, A., Herve, Y., Dorizon, S., Quantin-Nataf, C., Benedix, W-S., Schwenzer, S., Pettinelli, E., Heggyy, E., Herique, A., Berthelier, J-J., Kofman, W., Vago, J. L., Hamran, S-E., and the WISDOM team, 2017. The WISDOM radar: unveiling the subsurface beneath the ExoMars rover and identifying the best locations for drilling. Astrobiology, Mary Ann Liebert 17 (6–7), 565–584.

Clifford, S. M., Parker, T.J., 2001. The evolution of the Martian hydrosphere: Implications for the fate of a primordial ocean and the current state of the northern plains. Icarus, 154, 40–79.

Clifford, S. M., Lasue, J., Heggy, E., Boisson, J., McGovern, P., and Max, M. D., 2010. Depth of the Martian cryosphere: Revised estimates and implications for the existence and detection of subpermafrost groundwater. Journal of Geophysical Research 115, E07001, doi:10.1029/2009JE003462.

Colantuono, Luca; Baliva, Antonio; Lauro, Sebastian; Mattei, Elisabetta; Marinangeli, Lucia; Pettinelli, Elena; Seu, Roberto 2014. Mars: electric properties of clay materials in martian-like conditions to refine radar investigation. EGU General Assembly 2014, held 27 April - 2 May, 2014 in Vienna, Austria, id.14382

Conway, S.J., Hovius, N., Barnie, T., Besserer, J., Le Mouélic, S., Orosei, R., Read, N.A., 2012. Climate-driven deposition of water ice and the formation of mounds in craters in Mars' north polar region. Icarus 220. 174–193.

This project has received funding from the European Union's Horizon 2020 research and innovation programme under MSCA-RISE2020 grant agreement No 101007973.

Cook, J.C. (1957). Radar transparencies of mine and tunnel rocks. Geophisics, Vol. 40, n°. 5, p. 865-885.

Dickson, James L.; Head, James W.; Goudge, Timothy A.; Barbieri, Lindsay 2015. Recent climate cycles on Mars: Stratigraphic relationships between multiple generations of gullies and the latitude dependent mantle. Icarus, Volume 252, p. 83-94.

Fanara, L.; Gwinner, K.; Hauber, E.; Oberst, J. 2016. Mass MOVEMENTS' Detection in Hirise Images of the North Pole of Mars. ISPRS International Archives of the Photogrammetry, Remote Sensing and Spatial Information Sciences, Volume XLI-B4, 2016, pp.383-384.

Ferro, A (2011). Advanced methods for the analysis of radar sounder and vhr sar signals. 2011.

GeoSci. Developpers, (2017) Geophysics for practicing geoscientists https://gpg.geosci.xyz/content/GPR/GPR_fundamental_principles.html. (last view 31/05/2021)

Goossens, S., Sabaka, T.J., Genova, A., Mazarico, E., Nicholas, J.B., and Neumann, G.A., 2017. Evidence for a low bulk crustal density for Mars from gravity and topography. Geophysical Research Letters 44, 7686–7694. doi:10.1002/2017gl074172.

Grima, C., Kofman, W., Mouginot, J., Phillips, R. J., Héique, A., Biccari, D., Seu, R., and Cutigni, M., 2009. North polar deposits on Mars: Extreme purity of the water ice. Geophysical Research Letters 36, L03203 doi:10.1029/2008GL036326.

Grima, C. (2011) Etude de la surface et de la subsurface de Mars par sondage radar. Analyse des données MRO/Sharad. Theses, Université de Grenoble. Français. NNT: 2011GRENU004. tel-00583703.

Grima, C., Kofman, W., Herique, A., Orosei, R., Seu, R., 2012. Quantitative analysis of Mars surface radar reflectivity at 20 MHz. Icarus 220 (2012) 84–99.

Gurnett D.A., Kirchner D.L., Huff R.L., Morgan, D. D., Persoon, A. M., Averkamp, T. F., Duru, F., Nielsen, E., Safaeinili, A., Plaut, J. J., Picardi, G., 2005. Radar soundings of the ionosphere of Mars. Science 310, 1929–1933.

Hamran S.E., Paige D.A., Amundsen, H. E. F., Berger, T., Brovoll, S., Carter, L., Damsgård, L., Dypvik, H., Eide, J., Eide, S., Ghent, R., Helleren, Ø., Kohler, J., Mellon, M., Nunes, D. C., Plettemeier, D., Rowe, K., Russell, P., Øyan, M. J., 2020. Radar Imager for Mars' Subsurface Experiment—RIMFAX. Space Science Reviews, 216, 128.

Harish; Vijayan, S.; Mangold, N.; Bhardwaj, Anil 2020. Water-Ice Exposing Scarps Within the Northern Mid-latitude Craters on Mars. Geophysical Research Letters, Volume 47, Issue 14, article id. e89057.

Head, J.W., Weiss, D.K., 2014. Preservation of ancient ice at Pavonis and ArsiaMons: tropical mountain glacier deposits on Mars. Planetary and Space Science 103, 331–338.

Hecht, M. H, Kounaves, S. P., Quinn, R.C., West, S. J., Young, M.M., Ming, D.C., Catling, D.C., Clark, B.C., Boynton, W.V., Hoffman, J., Deflores, L.P., Gospodinova, K., Kapit, J., and Smith, P. H., 2009. Detection of perchlorate and the soluble chemistry of martian soil at the Phoenix lander site. Science 325, 64–67 (2009). doi:10.1126/science.1172466.

Jordan R., Picardi G., Plaut J., Wheeler, K., Kirchner, D., Safaeinili, A., Johnson, W., Seu, R., Calabrese, D., Zampolini, E., Cicchetti, A., Huff, R., Gurnett, D., Ivanov, A., Kofman, W., Orosei, R., Thompson, T., Eden-

This project has received funding from the European Union's Horizon 2020 research and innovation programme under MSCA-RISE2020 grant agreement No 101007973.

hofer, P., Bombaci, O., 2009. The Mars express MARSIS sounder instrument. Planetary and Space Science, 57, 1975–1986. DOI: 10.1016/j.pss.2009.09.016

Langlais, B., Thébault, E., Houliez, A., Purucker, M.E., Lillis, R. J., 2019. A New Model of the Crustal Magnetic Field of Mars UsingMGS and MAVEN. Journal of Geophysical Research: Planets, 10.1029/2018JE005854.

Mège, D., and Masson, P., 1996. A plume tectonics model for the Tharsis province, Mars. Planet. Space Sci., 44, 12, 1499-1546, doi:10.1016/S0032-0633(96)00113-4.

Morgan, G. A.; Campbell, B. A.; Carter, L. M.; Plaut, J. J. 2011. SHARAD Investigation of the Interaction Between Volcanism and Deep Water Release in Elysium Planitia, Mars. American Geophysical Union, Fall Meeting 2011, abstract id.P31B-1711.

Mouginot, J., Pommerol, A., Kofman, W., Beck, P., Schmitt, B., Herique, A., Grima, C., Safaeinili, A., Plaut, J.J., 2010. The 3–5 MHz global reflectivity map of Mars by MARSIS/Mars Express: Implications for the current inventory of subsurface H2O. Icarus 210 (2010) 612–625.

Nerozzi, S.; Tober, B.; Holt, J. W.; Ortiz, M. 2020. Reconstructing the geologic history of Hebrus Valles and Hephaestus Fossae, Mars with SHARAD. American Geophysical Union, Fall Meeting 2020, abstract #P016-0004

Nunes D.C., Phillips R:J. 2006. Radar subsurface mapping of the polar layered deposits on Mars. J. Geophys. Res. Planets 111, E06S21, 10.1029/2005JE002609

Nunes, D. C., S. E. Smrekar, A. Safaeinili, J. Holt, R. J. Phillips, R. Seu, and B. Campbell (2010), Examination ofgully sites on Mars with the shallow radar,J. Geophys. Res.,115, E10004, doi:10.1029/2009JE003509.

Nunes, D. C.; Fisher, B.; Smrekar, S. E.; Plaut, J. J.; Holt, J. W.; Phillips, R. J.; Seu, R.; Head, J. W. 2009. Pedestal crater deposits as seen by SHARAD. American Geophysical Union, Fall Meeting 2009, abstract id.P13B-1277.

Orosei, R., Lauro, S. E., Pettinelli, E., Cicchetti, A., Coradini, M., Cosciotti, B., Di Paolo, F., Flamini, E., Mattei, E., Pajola, M., Soldovieri, F., Cartacci, M., Cassenti, F., Frigeri, A., Giuppi, S., Martufi, R., Masdea, A., Mitri, G., Nenna, C., Noschese, R., Restano, M., Seu, R.,2018. Radar evidence of subglacial liquid water on Mars. Science 361, 490–493.

Pérez-Cerquera, M.R., Colorado-Montaño, J.D., and Mondragón, I. (2017) Uav for landmine detection using sdr-based gpr technology. DOI: 10.5772/intechopen.69738.

Perry, M. R.; Putzig, N. E.; Bain, Z. M.; Crown, D. A.; Scheidt, S. P.; Nunes, D. E. 2019. Detection and Characterization of Intact Lava Tubes on the Western Flank of Alba Mons in Mars Reconnaissance Orbiter Shallow Radar (SHARAD) Data. Ninth International Conference on Mars, held 22-25 July, 2019 in Pasadena, California. LPI Contribution No. 2089, id.6405

Petersen, E.; Holt, J. W.; Levy, J. S.; Lalich, D. 2017. Variability in radar returns from Martian debris-covered glaciers attributed to surface debris layer roughness and composition: implications for the regional distribution of massive subsurface ice and near-surface pore-filling ice. American Geophysical Union, Fall Meeting 2017, abstract #P43C-2889

Petrenko, V.F., Whitworth, R.W., 1999. Physics of Ice. Oxford University Press, New York.

This project has received funding from the European Union's Horizon 2020 research and innovation programme under MSCA-RISE2020 grant agreement No 101007973.

Phillips, R. J.; Davis, B. J.; Byrne, S.; Campbell, B. A.; Carter, L. M.; Haberle, R. M.; Holt, J. W.; Kahre, M. A.; Nunes, D. C.; Plaut, J. J.; Putzig, N. E.; Smith, I. B.; Smrekar, S. E.; Tanaka, K. L.; Titus, T. N. 2010. SHARAD Finds Voluminous CO2 Ice Sequestered in the Martian South Polar Layered Deposits. American Geophysical Union, Fall Meeting 2010, abstract id.P34A-01.

Plaut, J.J., Picardi, G., Safaeinili, A., Ivanov A. B., Milkovich, S. M., Cicchetti, A., Kofman, W., Mouginot, J., Farrell, W. M., Philips, R. J., Clifford, S. M., Frigeri, A., Orosei, R., Federico, C., Williams, I, Gournett, D. A., Nielsen, E., Hagfors, T., Heggy, E., Stofan, E., Plettemeier, D., Watters, T. R., Leuschen, C. J., Edenhofer, P., 2007. Subsurface Radar sounding of the South Polar Layered Deposits of Mars. Science 316, 92–95.

Plaut J.J., Safaeinili A., Holt J.W., Phillips, R. J., Head, J. W., Seu, R., Putzig, N. E., Frigeri, A., 2009. Radar evidence for ice in lobate debris aprons in the mid-northern latitudes of Mars. Geophysical Research Letters, 36, DOI:10.1029/ 2008GL036379.

Plaut, J.J. 2020. Radar Remote Sensing of Planetary Bodies, in: Bishop, J.L., Bell III, J.F., Moersch, J.E., 2020. Remote compositional analysis, (604-623 p.) Cambridge University Press.

Porcello, L.J., et al. (1974). 'The Apollo Lunar Sounder Radar System. Proceedings of the IEEE, 62 (6).

Putzig, N. E. 2017. A SHARAD's Eye View of Martian Dunes. Fifth International Planetary Dunes Workshop, Proceedings of the conference held 16-19 May, 2017 in St. George, Utah. LPI Contribution No. 1961, 2017, id.3054.

Putzig N.E. Hoover R.H. 2018. Searching for buried water ice in martian dunes with radar and thermal data.49th Lunar and Planetary Science Conference 2362.

Safaeinili, A., Kofman, W., Mouginot, J., Gim, Y., Hérique, A., Ivanov, A., Plaut, J., Picardi, G., 2007. Estimation of the total electron content of the Martian ionosphere using radar sounder surface echoes. Geophysical Research Letters, American Geophysical Union, 2007, 34 (23), pp.L23204.

Scott, D.H.; Dohm, J.M.; Zimbleman, J.R., 1998. Geologic Maps of Pavonis Mons, Mars. USGS, I-2561.

Seu R., Phillips R.J., Biccari D., Orosei, R., Masdea, A., Picardi, G., Safaeinili, A., Campbell, B. A., Plaut, J. J., Marinageli, L., Smrekar, S. E., Nunes, D. C., 2007. SHARAD sounding radar on the Mars Reconnaissance Orbiter. Journal of Geophysical Research, 112, DOI:10.1029/2006JE002745.

Shoemaker, E. S.; Baker, D. M. H.; Carter, L. M. 2018. Radar Sounding of Open Basin Lakes on Mars. Journal of Geophysical Research: Planets, Volume 123, Issue 6, pp. 1395-1406.

Shoemaker, E. S.; Carter, L. M.; Garry, W. B.; Morgan, G. A. 2020. Radar sounding of lava flows northwest of ascraeus mons, mars. 51st Lunar and Planetary Science Conference, held 16-20 March, 2020 at The Woodlands, Texas. LPI Contribution No. 2326, 2020, id.2752Smith I.B., Putzig N.E., Holt J.W., Phillips R.J. 2016. An ice age recorded in the polar deposits of Mars. Science Vol. 352, Issue 6289, pp. 1075-1078. DOI: 10.1126/science.aad6968

Smrekar, S. E., Lognonné, P., Spohn, T., Banerdt, W. B., Breuer, D., Christensen, U., Dehant, V., Drilleau, M., Folkner, W., Fuji, N., Garcia, R. F., Giardini, D., Golombek, M., Grott, M., Gudkova, T., Johnson, C., Khan, A., Langlais, B., Mittelholz, A., Mocquet, A., Myhill, R., Panning, M., Perrin, C., Pike, T., Plesa, A. C., Rivoldini, A., Samuel, H., Stahler, S. C., Van Driel, M., Van Hoolst, T., Verhoeven, O., Weber, R., Wieczorek, M., 2019. Premission InSights on the Interior of Mars. Space Science Reviews, 215(1). doi:10.1007/s11214-018-0563-9.

This project has received funding from the European Union's Horizon 2020 research and innovation programme under MSCA-RISE2020 grant agreement No 101007973.

Stillman D.E., Olhoeft G.R. 2006. Electromagnetic properties of Martian analog minerals at radar frequencies and Martian temperatures. 37th Lunar and Planetary Science, abstract 2002.

Stillman D.E., Olhoeft G.R. 2008. Frequency and temperature dependence in electromagnetic properties of Martian analog minerals. Journal of Geophysical Research Atmospheres 113(E9), DOI: 10.1029/2007JE002977

Stuurman C.M., Osinski G.R., Holt J.W., Levy, J. S., Brothers, T. C., Kerrigan, M., Campbell, B. A., 2016. SHARAD detection and characterization of subsurface water ice deposits in Utopia Planitia, Mars. Geophysical Research Letters, 43, 9484–9491.

Tsige, Meaza; Ruiz, Javier; del Río, Ian A.; Jiménez-Díaz, Alberto2016. Modeling of Landslides in Valles Marineris, Mars, and Implications for Initiation Mechanism. Earth, Moon, and Planets, Volume 118, Issue 1, pp.15-26

Watters, Thomas R.; Leuschen, Carl J.; Plaut, Jeffrey J.; Picardi, Giovanni; Safaeinili, Ali; Clifford, Stephen M.; Farrell, William M.; Ivanov, Anton B.; Phillips, Roger J.; Stofan, Ellen R. 2006. MARSIS radar sounder evidence of buried basins in the northern lowlands of Mars. Nature, Volume 444, Issue 7121, pp. 905-908.

Whitten, Jennifer L.; Campbell, Bruce A.; Plaut, Jeffrey J. 2020. The Ice Content of the Dorsa Argentea Formation from Radar Sounder Data. Geophysical Research Letters, Volume 47, Issue 23, article id. e90705

Williams, Kevin K.; Greeley, Ronald 2004. Measurements of dielectric loss factors due to a Martian dust analog. Journal of Geophysical Research, Volume 109, Issue E10, CiteID E10006

Watters, T. R.; Campbell, B.; Carter, L.; Leuschen, C. J.; Plaut, J. J.; Picardi, G.; Orosei, R.; Safaeinili, A.; Clifford, S. M.; Farrell, W. M.; Ivanov, A. B.; Phillips, R. J.; Stofan, E. R., 2007. Radar Sounding of the Medusae Fossae Formation Mars: Equatorial Ice or Dry, Low-Density Deposits? Science. 318 (5853): 1125–1128.

Wilson, L., and Head, J. W., 1994. Mars: Review and analysis of volcanic eruption theory and relationships to observed landforms. Reviews of Geophysics 32, 221–1263.

Wilson, J. T.; Eke, Vincent R.; Massey, Richard J.; Elphic, Richard C.; Feldman, William C.; Maurice, Sylvestre; Teodoro, Luís F.A., 2018. Equatorial locations of water on Mars: Improved resolution maps based on Mars Odyssey Neutron Spectrometer data. Icarus. 299: 148–160.

Xiong, Siting; Tao, Yu; Persaud, Divya M.; Campbell, Jacqueline D.; Putri, Alfiah Rizky Diana; Muller, Jan-Peter 2021. Stratigraphy and Buried Channels Over Central Elysium Planitia, Mars. Earth and Space Science, Volume 8, Issue 1, article id. e00968

Zhang Z. Hagfors T., Nielsen E., Picardi G., Mesdea A. 2008. Dielectric properties of the Martian south polar layered deposits: MARSIS data inversion using Bayesian inference and genetic algorithm. Journal of Geophysical Research Atmospheres 113(E5), DOI: 10.1029/2007JE002941

This project has received funding from the European Union's Horizon 2020 research and innovation programme under MSCA-RISE2020 grant agreement No 101007973.

END OF REPORT

This project has received funding from the European Union's Horizon 2020 research and innovation programme under MSCA-RISE2020 grant agreement No 101007973.